

Short communication

Alkali titanate nanobelts-supported Pd catalysts for room temperature formaldehyde oxidation



Li Zhou^a, Shuren He^a, Yuanhua Sang^b, Xiaomei Zhang^a, Hong Liu^b, Chuancheng Jia^{c,*}, Xiaohong Xu^{a,*}

^a School of Chemistry and Chemical Engineering, Shandong University, Jinan, Shandong 250100, China

^b State Key Laboratory of Crystal Materials, Shandong University, Jinan, Shandong 250100, China

^c International Frontier Center of Single-Molecule Science, College of Electronic Information and Optical Engineering, Nankai University, Tianjin 300350, China

ARTICLE INFO

Keywords:

Heterogeneous catalysis

Palladium

Alkali metal

Titanate nanobelt

HCHO oxidation

ABSTRACT

Pd clusters supported on alkali titanate (Na- and K-titanate) nanobelts were synthesized and investigated for the catalytic HCHO oxidation at room temperature. The presence of interlayer alkali metal promoted the dispersion of Pd species and simultaneously made the Pd clusters more negatively charged, thus enhancing the catalytic performance for HCHO oxidation reaction at room temperature. Especially, Pd clusters with the smaller size and larger quantity of Pd⁰ supported on K-titanate nanobelts contributed to higher catalytic activity and stability, where nearly complete HCHO oxidation was achieved with a Pd loading of 1 wt% at ambient temperature.

1. Introduction

Formaldehyde (HCHO) as a primary indoor air pollutant with high carcinogenicity and mutagenicity [1,2] has received considerable attention for its removal in reducing public health risk. The characteristics of an ideal process for indoor HCHO purification consist of non-secondary pollutant production, convenience, and low energy consumption. The catalytic oxidation was shown to meet this requirement, in which HCHO can be completely oxidized over well-designed catalysts at room temperature producing only H₂O and CO₂ as clean products [3,4]. Efficient catalysts for room-temperature HCHO oxidation are mainly supported noble metal catalysts, including Pt, Au, Pd and Ag [5–9]. Their catalytic performances on HCHO oxidation are strongly correlated with the use of reducible supports because of the remarkable influence of strong metal-support interaction (SMSI) on intrinsic properties of metal species, such as chemical state and particle sizes [10,11].

Regarding catalytic oxidation of HCHO over supported noble metal catalysts, titanium dioxide (TiO₂) is one of the most widely investigated supports [5,7]. It has been found that the addition of alkali metal ions (Na⁺ and K⁺) can significantly enhance the catalytic performances of TiO₂ supported noble metal catalysts, such as Ag, Pt and Pd [12–15]. He et al. [16] reported that the addition of Na⁺ ions to Pt/TiO₂ catalyst can markedly improve the dispersion of Pt species, thus intensifying the catalytic performance. Similarly, such enhancement effect of alkali metal ions has also been reported for Pd-based catalysts [17,18]. With

the addition of Na⁺ species, the HCHO oxidation activity of catalyst is highly improved as a result of the formation of highly dispersed and negatively charged Pd species [14,18]. However, there is no yet a general mechanism to explain satisfactorily the promoting effect of alkali metal species on HCHO catalytic oxidation reaction. In most cases, it is postulated that the presence of alkali metal salts can provide OH⁻ ions which contribute to the enhanced activity of catalysts, instead of additional alkali metal ions. Moreover, the alkali metal additions usually lead to more negatively charged and dispersed metal species [11,17]. The negatively charged Pd species is beneficial to H₂O activation and oxygen chemisorption, and highly dispersed Pd clusters/nanoparticles would bring more active sites [18,19].

At the present time, most studies have focused on the external addition of alkali metals, while few reports involved using layered alkali metal titanates directly as supports in noble metal catalysts. Sodium and potassium titanate are layered alkali metal titanates, where TiO₆ octahedrons are joined together to form two-dimensional planes stacking layer by layer, between which the alkali metal ions are located in the crystal (Fig. S1, ESI) [20]. Consequently, Na-titanate and K-titanate nanobelts (NTO-NB and KTO-NB) can be easily synthesized by hydrothermal treatment of TiO₂ precursors in concentrated alkaline solution due to their layered structure [21,22]. These one-dimensional nanostructures also intrinsically possess Na⁺ or K⁺ ions. More significantly, the hydrothermally synthesized NTO-NB and KTO-NB have high specific surface areas and clean surface with uniform defects, on

* Corresponding authors.

E-mail addresses: jiacc@chem.ucla.edu (C. Jia), xhxu@sdu.edu.cn (X. Xu).

<https://doi.org/10.1016/j.catcom.2020.106034>

Received 16 December 2019; Received in revised form 30 April 2020; Accepted 1 May 2020

Available online 06 May 2020

1566-7367/ © 2020 Elsevier B.V. All rights reserved.

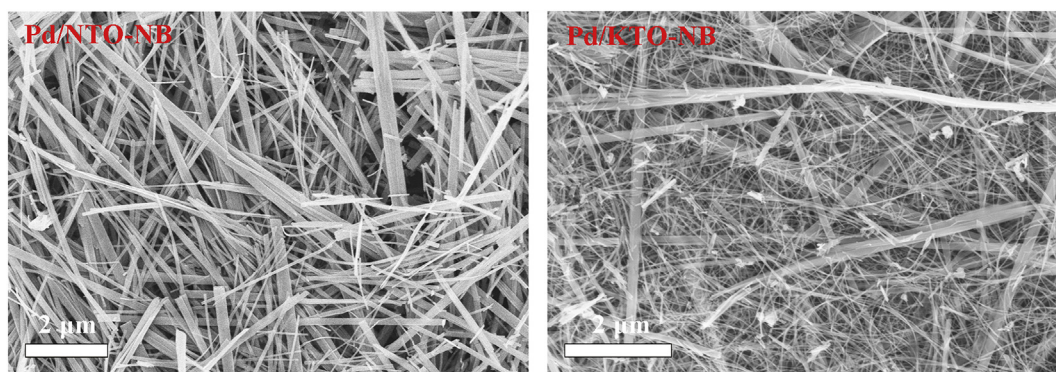


Fig. 1. The SEM images of Pd/NTO-NB and Pd/KTO-NB samples.

which the deposition of uniform and well dispersed noble metal nanoparticles and clusters can be obtained [23,24].

In this work, Na-titanate and K-titanate were synthesized and used to prepare supported palladium catalysts (code: Pd/NTO-NB, Pd/KTO-NB) by a facile deposition-precipitation method. The results showed that Pd/NTO-NB and Pd/KTO-NB catalysts are much more efficient for HCHO oxidation at room temperature compared to TiO₂ nanobelts (TiO₂-NB) supported palladium catalyst (Pd/TiO₂-NB), where Pd/KTO-NB catalyst provided the best catalytic performance.

2. Experimental

2.1. Synthesis of Pd_x/M ($x = 0.5, 1 \text{ wt\%}$, $M = \text{KTO-NB, NTO-NB and TiO}_2\text{-NB}$) catalysts

Firstly, NTO-NB was synthesized by a typical hydrothermal process [22]. KTO-NB and H₂Ti₃O₇ nanobelt (HTO-NB) were then synthesized through hydrothermal treating of NTO-NB in KOH solution and acid-treating of NTO-NB, respectively [22,25]. The detailed experimental procedure is provided in the Electronic Supporting Information (ESI).

Pd_x/NTO-NB catalysts were prepared by the deposition-precipitation method, using PdCl₂ as the precursor compound. NTO-NB was dispersed evenly in PdCl₂ solution under stirring, and appropriate amount of urea was then dropped to adjust the pH of precursor solution (urea/Pd = 200 M ratio, 100 mL). Next, the suspension was thermostatically kept at 80 °C for 4 h under vigorous magnetic stirring in the dark. The resulting product was filtered and washed with ultrapure water for several times, then dried in air at 80 °C for 12 h, and then treated at 400 °C for additional 2 h with a 5 °C min⁻¹ heating rate under pure H₂ gas flow.

Pd_x/KTO-NB and Pd_x/TiO₂-NB catalysts were synthesized by the same process as the synthesis of Pd_x/NTO-NB, except using KTO-NB and HTO-NB as support, respectively.

2.2. Catalysts characterization

The metal loading in the as-prepared catalysts was analysed using inductively coupled plasma atomic emission spectroscopy (ICP-AES). Powder X-ray diffraction (XRD) analysis of the samples was conducted on a PANalytical X'pert3 powder diffractometer using Cu K α radiation. Scanning electron microscope (SEM) and energy dispersion spectra (EDS) were acquired on a Zeiss Gemini300 scanning electron microscope. Transmission electron microscopy (TEM) and high-resolution transmission electron microscopy (HRTEM) images were obtained with a JOEL JEM 2100 microscope. Brunauer-Emmett-Teller (BET) surface areas of the samples were measured by nitrogen adsorption-desorption isotherms at -196 °C using a Builder SSA-4200 apparatus. Diffuse reflectance infrared Fourier transform spectroscopy (DRIFTS) measurements were carried out on a BRUKER VERTEX-70 FTIR. X-ray photoelectron spectroscopy (XPS) measurements were carried out with a

Thermo ESCALAB 250 X-ray photoelectron spectrometer.

2.3. Catalytic activity tests

Before catalytic testing and characterization of a given solid, the as-synthesized solid samples were treated in pure H₂ gas flow at 400 °C for 2 h, and marked as Pd/KTO-NB, Pd/NTO-NB and Pd/TiO₂-NB, respectively. The samples pretreated in simulated air (O₂/N₂ = 21:79) are denoted as PdO/KTO-NB, PdO/NTO-NB and PdO/TiO₂-NB, respectively. The fresh catalyst samples before any gas/thermal treatment are marked as Pd/KTO-NB-F, Pd/NTO-NB-F and Pd/TiO₂-NB-F, respectively. The catalytic oxidation of HCHO was carried out in a quartz tubular (i.d. = 6 mm) fixed-bed reactor under 1 atm pressure at room temperature (25 °C). Gaseous HCHO was produced by flowing N₂ gas via pyrolysis of paraformaldehyde in a water bath thermostatically held at 28 °C. Water was added in a vaporization furnace by an injection pump with the flow of 0.30 mL min⁻¹, and evaporated at 120 °C. Thus, the feed gas contained 140 ppm HCHO, simulated air (O₂/N₂ = 21:79) and water vapor (25% relative humidity). The total flow rate was 50 mL min⁻¹ and the gas hourly space velocity (GHSV) was 20,000 h⁻¹. The gas flow rate was regulated by a mass flow controller. The HCHO concentration in the feed gas and exit gas streams was determined by the phenol reagent colorimetric method (GBT18204.2-2014, china).

3. Results and discussion

As expected, typical Na-titanate nanobelts with a width of 50–200 nm and length of up to dozens of micrometers were synthesized by the hydrothermal method. A very similar one-dimensional morphology is seen for acidified H₂Ti₃O₇ nanobelts, Pd/NTO-NB and Pd/TiO₂-NB samples (Fig. 1, Fig. S2 in ESI). Powder XRD characterization shows that the diffraction peaks of Na₂Ti₆O₁₃ and Na₂Ti₃O₇ appear in the pattern of Pd/NTO-NB sample after H₂-treatment at 400 °C (Fig. S3, ESI). For the Pd/TiO₂-NB sample, the observed diffraction peaks are all attributed to TiO₂ (B) (Fig. S3, ESI), a dehydrated product of H₂Ti₃O₇ at lower calcination temperature. Pd/KTO-NB sample displays a different morphology, composed of narrow nanobelts mixed with incompletely splitting wide nanobelts (Fig. 1). This indicates that the applied hydrothermal treatment in KOH solution resulted in Na-titanate nanobelts splitting into narrow K-titanate nanobelts due to bulk phase transformation [21]. The transformation process is incomplete. For Pd₁/KTO-NB sample, K₂Ti₆O₁₃ peaks appear in the XRD pattern but no Na₂Ti₆O₁₃ peaks appear, and weaker Na₂Ti₃O₇ reflections still can be observed (Fig. S3, ESI). For all samples, no diffraction peaks of metallic Pd or PdO were detected, due to the low metal loading used and the high dispersion of Pd species formed. ICP-AES analysis gave a 0.34–0.75 wt% Pd-loading for the different samples (Table S1, ESI).

As shown in SEM images of Pd/NTO-NB, Pd/TiO₂-NB and Pd/KTO-NB samples (Fig. 1 and Fig. S2 in ESI), their one-dimensional

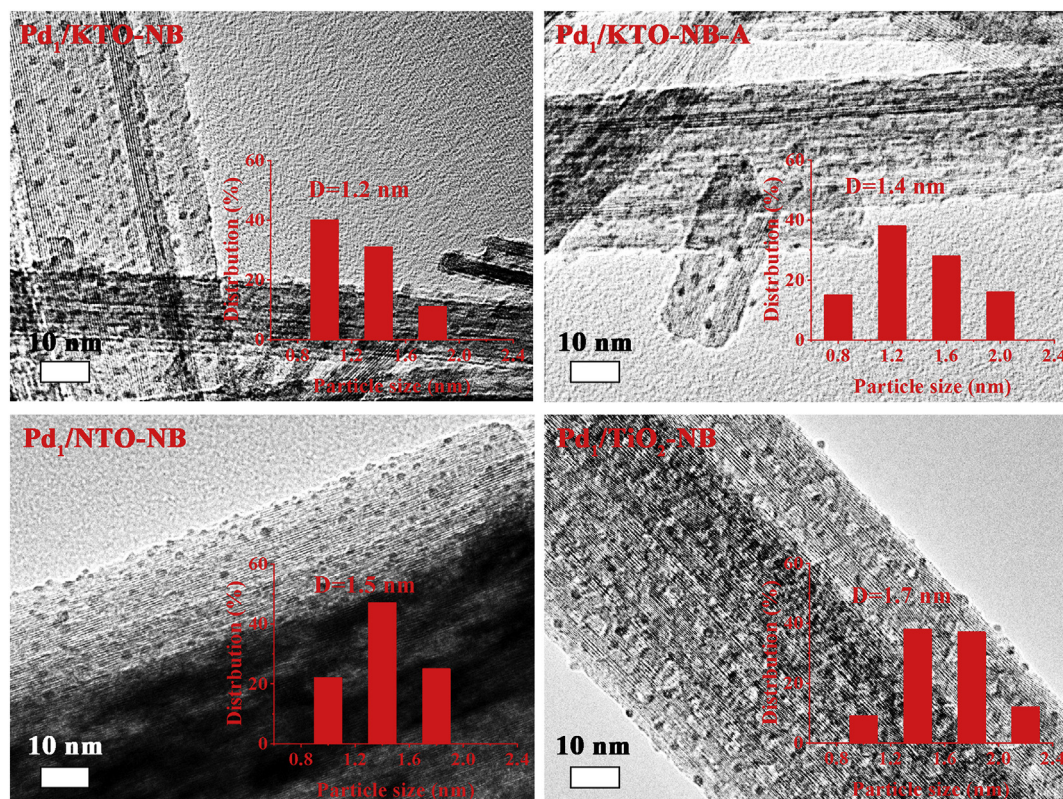


Fig. 2. Typical TEM images and the corresponding cluster size distributions of as-prepared Pd₁/KTO-NB, Pd₁/NTO-NB, Pd₁/TiO₂-NB and Pd₁/KTO-NB after reaction (Pd₁/KTO-NB-A).

nanostuctures with large aspect ratio enable the formation of a high porosity structure by overlapping with each other. Such uniform and highly porous structures are favorable for improving mass transfer rates in a heterogeneous catalytic reaction process. The HRTEM images of Pd₁/KTO-NB, Pd₁/NTO-NB and Pd₁/TiO₂-NB all show that a large amount of tiny Pd clusters is uniformly distributed on nanobelts, and their corresponding average diameters are ~1.2, ~1.5 and ~1.7 nm, respectively (Fig. 2). In particular, the Pd clusters with size less than 1 nm are more numerous in Pd₁/KTO-NB and Pd₁/NTO-NB catalysts compared to Pd₁/TiO₂-NB catalyst. It demonstrates that the existence of interlayer Na⁺ and K⁺ ions prompt the dispersion of Pd species on the KTO-NB and NTO-NB supports. In addition, DRIFTS spectra of CO adsorption presented a larger proportion of linear CO IR band for the Pd₁/NTO-NB than Pd₁/TiO₂-NB catalyst, also suggesting for a better dispersion of Pd species on the NTO-NB support (Fig. S4, ESI) [26]. Such result agrees with previous findings that the addition of Na⁺ ions into Pd/TiO₂ can markedly increase the dispersion of Pd nanoparticles [17,18]. Pd₁/KTO-NB catalyst gave the smallest Pd clusters in size, which is related to the much smaller diameter of KTO-NB. The measured BET surface area of Pd₁/KTO-NB (~55 m² g⁻¹) is significantly larger than those of Pd₁/NTO-NB (~36 m² g⁻¹) and Pd₁/TiO₂-NB (~23 m² g⁻¹). Such KTO-NB surface has more active sites for Pd clusters nucleation, and is in favor of the formation of smaller clusters in size. On the other hand, the different surface electron structure of the three nanobelts may also influence the dispersion of Pd species due to strong interactions between Pd species and the support.

The impact of support on the electron structure of Pd/KTO-NB, Pd/NTO-NB and Pd/TiO₂-NB catalysts was investigated by XPS analysis, and results are presented in Fig. 3. For all three as-prepared samples, Pd 3d XPS peak can be deconvoluted into two parts, metallic Pd and PdO, demonstrating that Pd clusters are comprising of metallic Pd as main component along with PdO. The latter comes from either the incomplete hydrogen reduction of Pd²⁺ [27] or the inevitable oxidation

of reactive Pd clusters when exposed to the air during sample handling. In more detail, for Pd₁/TiO₂-NB sample, Pd 3d_{5/2} spectra can be fitted to two peaks of 335.5 and 337.0 eV, identified as Pd⁰ and PdO, respectively [28,29]. Similarly, the binding energies of Pd 3d_{5/2} in Pd₁/NTO-NB and Pd₁/KTO-NB can also be deconvoluted into two peaks, ca. 335.1 and 337.6 eV, as well as 335.0 and 336.3 eV, corresponding to Pd⁰ and PdO respectively [14,17]. The lower Pd⁰ binding energies and higher Pd⁰/PdO ratio (Table S2, ESI) appeared in Pd₁/NTO-NB and Pd₁/KTO-NB indicate that Pd clusters on NTO-NB and KTO-NB are more negatively charged than those on TiO₂-NB. This result might be related to the electron donating effect of interlayer alkali metals [18,30]. As regards Pd₁/NTO-NB and Pd₁/KTO-NB, there is a charge transfer from alkali metal to the TiO₆ octahedron planes which leads to an increase in the electron density at Ti atoms [17,31]. Indeed, the binding energies of Ti 2p in both Pd₁/NTO-NB and Pd₁/KTO-NB are negatively shifted to 458.3 eV in comparison to that in Pd₁/TiO₂-NB (458.6 eV). This electron donating effect of interlayer alkali metals could then be transferred to Pd species, making Pd clusters more negatively charged.

The as-synthesized one-dimensional KTO-NB, NTO-NB and TiO₂-NB supported palladium clusters were applied in the room temperature HCHO oxidation, and results are shown in Fig. 4. Evidently, all three catalysts can effectively catalyze HCHO oxidation at ambient temperature (Fig. 4a). The catalytic activities are attributed to the presence of Pd species, because pure KTO-NB, NTO-NB and TiO₂-NB showed no activity in this reaction. Pd₁/KTO-NB exhibited the best catalytic performance, and a HCHO conversion larger than 97% was achieved at room temperature. Pd₁/NTO-NB, giving ~90% HCHO conversion after 7 h of reaction, also is more active than Pd₁/TiO₂-NB, showing ~48% conversion. The same dependence of activity on support was observed on the 0.5 wt% Pd loading samples. A conversion of ~85% and ~70% of HCHO was respectively achieved over Pd_{0.5}/KTO-NB and Pd_{0.5}/NTO-NB after 7 h of reaction, while a lower conversion of ~25% was

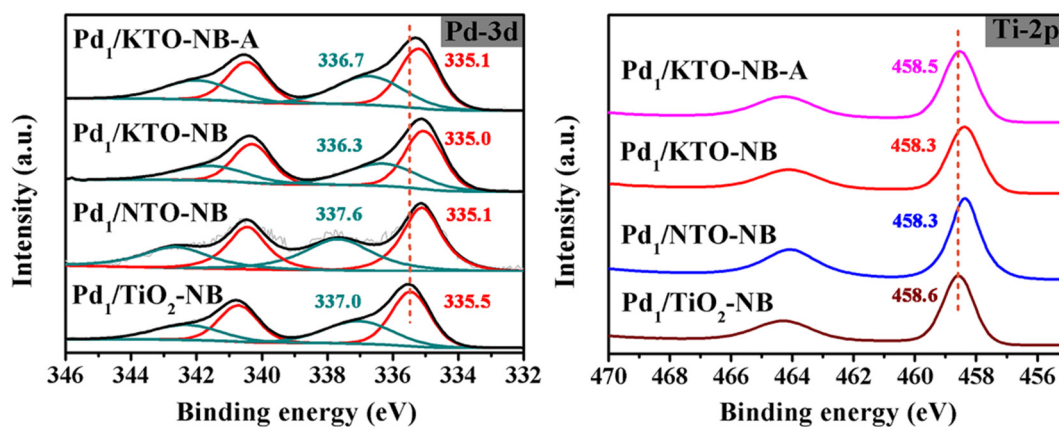


Fig. 3. XPS spectra of Pd 3d and Ti 2p in as-prepared Pd₁/NTO-NB, Pd₁/TiO₂-NB, Pd₁/KTO-NB and Pd₁/KTO-NB after 30 h reaction (Pd₁/KTO-NB-A).

obtained on Pd_{0.5}/TiO₂-NB. The higher activity observed in Pd/KTO-NB and Pd/NTO-NB than in Pd/TiO₂-NB can be attributed to the interlayer Na⁺ and K⁺ ions in NTO-NB and KTO-NB. As discussed above, for Pd species in Pd/KTO-NB and Pd/NTO-NB catalysts, the existence of Na⁺ and K⁺ ions increases their dispersion and makes them more negatively charged. The best catalytic performance of Pd/KTO-NB catalysts largely originates from their smallest Pd clusters size and the largest Pd⁰/Pd ratio among the series of palladium catalysts tested. In general, smaller Pd nanoparticles have more abundant active sites which favor the dissociative adsorption of oxygen on the catalyst surface, and lead to higher HCHO oxidation rates [19,32]. On the other hand, the negatively charged Pd species could enhance the electron transfer from Pd to the π* orbital of O₂, further promoting O₂ adsorption and HCHO oxidation [18,30].

In order to further clarify the nature of catalytic active Pd species, the catalytic performances of O₂-pretreated PdO₁/KTO-NB, PdO₁/NTO-NB and PdO₁/TiO₂-NB samples were tested. Much lower HCHO conversions of ~30%, ~20% and ~8% were achieved, respectively (Fig. S5, ESI). Moreover, all the fresh Pd₁/TiO₂-NB-F, Pd₁/NTO-NB-F and Pd₁/KTO-NB-F samples without hydrogen reduction treatment also gave poor HCHO conversion, below ~20% (Fig. S5, ESI). This result agrees with the previous findings that metallic Pd is the catalytically active species in palladium catalysts for room temperature HCHO oxidation, and not Pd²⁺ ions or PdO species [18,33].

Pd/KTO-NB catalyst presented the highest catalytic stability among the three prepared palladium catalysts. Also, an almost complete HCHO conversion was achieved with a GHSV of 20,000 h⁻¹ and a HCHO inlet concentration of 140 ppm at ambient temperature, and this was maintained over 30 h time-on-stream (Fig. 4b). Furthermore, the used

Pd₁/KTO-NB catalyst kept this excellent catalytic activity in a second reaction cycle, where almost complete HCHO conversion was still observed (Fig. S6, ESI). Such high catalytic stability may relate to the capability of KTO-NB to stabilize small sized Pd clusters and metallic Pd species. As shown in Fig. 2b, for the Pd₁/KTO-NB catalyst underwent 30 h of reaction, the mean diameter of Pd clusters increased slightly from ~1.2 to ~1.4 nm, suggesting a weaker agglomeration of Pd clusters during reaction. The almost unchanged Pd cluster size in Pd₁/KTO-NB catalyst before and after reaction can be ascribed to the strong interaction between Pd species and KTO-NB. This strong interactions makes the Pd clusters in Pd₁/KTO-NB catalyst most negatively charged and smallest-sized. Also, the latter catalyst showed best sintering resistance among the three catalysts.

In comparison, Pd₁/NTO-NB and Pd₁/TiO₂-NB catalysts showed a more significant increase in Pd clusters size during reaction, and the mean diameter of Pd clusters increased from 1.5 and 1.7 nm to 2.1 and 2.3 nm after reaction for 30 h, respectively (Fig. S7, ESI). The catalytic activity of these two solids presented a distinct decrease with reaction time (Fig. 4b). On the other hand, the XPS analysis revealed that the binding energy of Pd⁰ in the used Pd₁/KTO-NB catalyst (Pd/KTO-NB-A) presents a little positive shift, and the PdO content slightly increased from 39.54 to 39.64% (Table S2, ESI). This result indicates that the Pd clusters on K-titanate nanobelts could keep their electronic structure almost unchanged upon 30 h of continuous reaction, demonstrating a high stability of metallic Pd species during reaction.

4. Conclusions

In summary, supported palladium catalysts were prepared by the

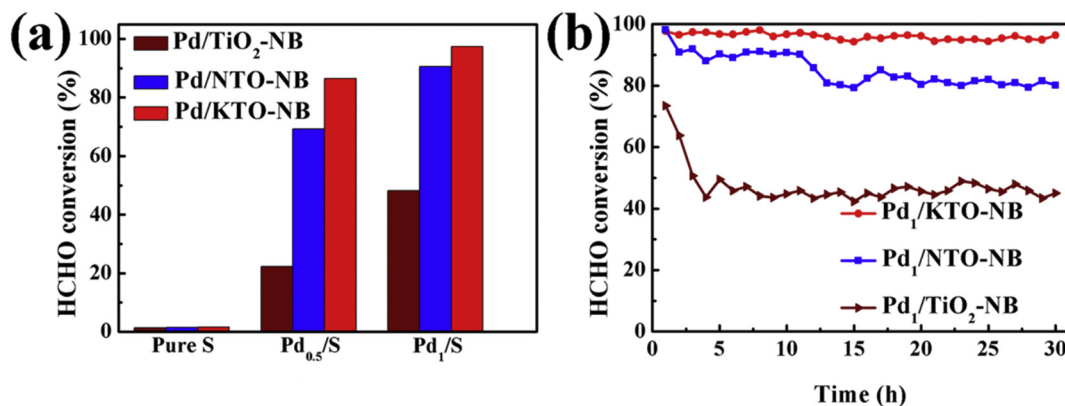


Fig. 4. (a) The comparison of HCHO oxidation over pure S, Pd_{0.5}/S and Pd₁/S catalysts (S = TiO₂-NB, NTO-NB and KTO-NB). (b) Catalytic stability test of Pd₁/TiO₂-NB, Pd₁/NTO-NB and Pd₁/KTO-NB catalysts. Reaction conditions: HCHO concentration 140 ppm, 21/79 of O₂/N₂, total flow rate 50 mL min⁻¹, catalysts of 50 mg, reaction temperature 25 °C, GHSV = 20,000 h⁻¹.

deposition-precipitation method using K-titanate, Na-titanate and TiO₂ nanobelts as supports. The presence of interlayer alkaline metal could significantly promoted the dispersion of Pd species on NTO-NB and KTO-NB carriers and made Pd clusters negatively charged simultaneously in comparison with the TiO₂-NB support, which contributed to the enhancement of catalytic performance for the room temperature HCHO oxidation reaction. Especially, when KTO-NB is formed by introducing K⁺ ions substituting the Na⁺ in NTO-titanate, the smallest sized and more negatively charged Pd clusters were obtained, which gave the highest catalytic activity and stability. This suggests that metallic Pd should be the active species in these alkali titanate supported palladium catalysts. The use of one-dimensional alkali titanate nanostructures as supports may provide a new approach to construct high-efficiency noble metal catalysts.

Acknowledgements

We acknowledge primary financial support from the National Natural Science Foundation of China (21176144, 21977064, 51732007), the National Key Research and Development Program of China (2017YFE0102700), and the Science Fund for Distinguished Young Scholars of Shandong Province (ZR2019JQ16).

Declaration of Competing Interest

There are no conflicts to declare.

Appendix A. Supplementary data

Supplementary data to this article can be found online at <https://doi.org/10.1016/j.catcom.2020.106034>.

References

- [1] B. Szende, E. Tyihak, *Cell Biol. Int.* 34 (2010) 1273–1282.
- [2] G. Speit, O. Schmid, *Mutat. Res.* 613 (2006) 1–9.
- [3] J. Quiroz Torres, S. Royer, J.P. Bellat, J.M. Giraudon, J.F. Lamonier, *ChemSusChem* 6 (2013) 578–592.
- [4] J. Pei, J.S. Zhang, *Hvac & R Res.* 17 (2011) 476–503.
- [5] F. Xu, Y. Le, B. Cheng, C. Jiang, *Appl. Surf. Sci.* 426 (2017) 333–341.
- [6] J. Xu, Z. Qu, Y. Wang, B. Huang, *Catal. Today* 327 (2019) 210–219.
- [7] Y. Li, C. Zhang, J. Ma, M. Chen, H. Deng, H. He, *Appl. Catal. B* 217 (2017) 560–569.
- [8] R. Fang, M. He, H. Huang, Q. Feng, J. Ji, Y. Zhan, D.Y.C. Leung, W. Zhao, *Chemosphere* 213 (2018) 235–243.
- [9] L. Nie, J. Yu, M. Jaroniec, F.F. Tao, *Catal. Sci. Technol.* 6 (2016) 3649–3669.
- [10] A. Lewera, L. Timperman, A. Roguska, N. Alonso-Vante, *J. Phys. Chem. C* 115 (2011) 20153–20159.
- [11] Y. Chen, J. He, H. Tian, D. Wang, Q. Yang, *J. Colloid Interface Sci.* 428 (2014) 1–7.
- [12] B. Bai, J. Li, *ACS Catal.* 4 (2014) 2753–2762.
- [13] L. Nie, J. Yu, X. Li, B. Cheng, G. Liu, M. Jaroniec, *Environ. Sci. Technol.* 47 (2013) 2777–2783.
- [14] Y. Li, C. Zhang, H. He, *Catal. Today* 281 (2017) 412–417.
- [15] C. Li, K. Sivaranjani, J.M. Kim, *Catal. Today* 265 (2016) 45–51.
- [16] C. Zhang, F. Liu, Y. Zhai, H. Ariga, N. Yi, Y. Liu, K. Asakura, M. Flytzani-Stephanopoulos, H. He, *Angew. Chem. Int. Ed.* 51 (2012) 9628–9632.
- [17] Y. Li, C. Zhang, H. He, J. Zhang, M. Chen, *Catal. Sci. Technol.* 6 (2016) 2289–2295.
- [18] C. Zhang, Y. Li, Y. Wang, H. He, *Environ. Sci. Technol.* 48 (2014) 5816–5822.
- [19] B.-R. Chen, L.A. Crosby, C. George, R.M. Kennedy, N.M. Schweitzer, J. Wen, R.P. Van Duyne, P.C. Stair, K.R. Poeppelmeier, L.D. Marks, M.J. Bedzyk, *ACS Catal.* 8 (2018) 4751–4760.
- [20] R.H. Wang, Q. Chen, B.L. Wang, S. Zhang, L.M. Peng, *Appl. Phys. Lett.* 86 (2005) 133101.
- [21] B.L. Wang, Q. Chen, R.H. Wang, L.M. Peng, *Chem. Phys. Lett.* 376 (2003) 726–731.
- [22] T. Zhang, Q. Chen, L.-M. Peng, *Adv. Funct. Mater.* 18 (2008) 3018–3025.
- [23] Q. Jia, D. Zhao, B. Tang, N. Zhao, H. Li, Y. Sang, N. Bao, X. Zhang, X. Xu, H. Liu, *J. Mater. Chem. A* 2 (2014) 16292–16298.
- [24] Y. Guan, N. Zhao, B. Tang, Q. Jia, X. Xu, H. Liu, R.I. Boughton, *Chem. Commun.* 49 (2013) 11524–11526.
- [25] M. Mori, Y. Kumagai, K. Matsunaga, I. Tanaka, *Phys. Rev. B* 79 (2009) 144117.
- [26] L.K. Ouyang, P.-F. Tian, G.-J. Da, X.-C. Xu, C. Ao, T.-Y. Chen, R. Si, J. Xu, Y.-F. Han, *J. Catal.* 321 (2015) 70–80.
- [27] K. Otto, L.P. Haack, J.E. de Vries, *Appl. Catal. B* 1 (1992) 1–12.
- [28] L.M. Esteves, M.H. Brijaldo, F.B. Passos, *J. Mol. Catal. A Chem.* 422 (2016) 275–288.
- [29] L. Ouyang, P.-f. Tian, G.-j. Da, X.-C. Xu, C. Ao, T.-y. Chen, R. Si, J. Xu, Y.-F. Han, *J. Catal.* 321 (2015) 70–80.
- [30] G. Pekridis, N. Kaklidis, M. Konsolakis, E.F. Iliopoulou, I.V. Yentekakis, G.E. Marnellos, *Top. Catal.* 54 (2011) 1135–1142.
- [31] Y. Li, X. Chen, C. Wang, C. Zhang, H. He, *ACS Catal.* 8 (2018) 11377–11385.
- [32] B. Qiao, A. Wang, X. Yang, L.F. Allard, Z. Jiang, Y. Cui, J. Liu, J. Li, T. Zhang, *Nat. Chem.* 3 (2011) 634–641.
- [33] H. Huang, D.Y.C. Leung, *ACS Catal.* 1 (2011) 348–354.